

Hydride-Containing Models for the Active Site of the Nickel–Iron Hydrogenases

Bryan E. Barton and Thomas B. Rauchfuss*

*School of Chemical Sciences, University of Illinois at Urbana–Champaign,
Urbana, Illinois 61801*

Received June 17, 2010; E-mail: rauchfuz@uiuc.edu

Abstract: The [NiFe]-hydrogenase model complex NiFe(pdt)(dppe)(CO)₃ (**1**) (pdt = 1,3-propanedithiolate) has been efficiently synthesized and found to be robust. This neutral complex sustains protonation to give the first nickel–iron hydride [1H]BF₄. One CO ligand in [1H]BF₄ is readily substituted by organophosphorus ligands to afford the substituted derivatives [HNiFe(pdt)(dppe)(PR₃)(CO)₂]BF₄, where PR₃ = P(OPh)₃ ([2H]BF₄); PPh₃ ([3H]BF₄); PPh₂Py ([4H]BF₄, where Py = 2-pyridyl). Variable temperature NMR measurements show that the neutral and protonated derivatives are dynamic on the NMR time scale, which partially symmetrizes the phosphine complex. The proposed stereodynamics involve twisting of the Ni(dppe) center, not rotation at the Fe(CO)₂(PR₃) center. In MeCN solution, **3**, which can be prepared by deprotonation of [3H]BF₄ with NaOMe, is about 10⁴ stronger base than is **1**. X-ray crystallographic analysis of [3H]BF₄ revealed a highly unsymmetrical bridging hydride, the Fe–H bond being 0.40 Å shorter than the Ni–H distance. Complexes [2H]BF₄, [3H]BF₄, and [4H]BF₄ undergo reductions near –1.46 V vs Fc^{0/+}. For [2H]BF₄, this reduction process is reversible, and we assign it as a one-electron process. In the presence of trifluoroacetic acid, proton reduction catalysis coincides with this reductive event. The dependence of *i_c/i_p* on the concentration of the acid indicates that H₂ evolution entails protonation of a reduced hydride. For [2H]⁺, [3H]⁺, and [4H]⁺, the acid-independent rate constants are 50–75 s^{–1}. For [2H]⁺ and [3H]⁺, the overpotentials for H₂ evolution are estimated to be 430 mV, whereas the overpotential for the *N*-protonated pyridinium complex [4H₂]²⁺ is estimated to be 260 mV. The mechanism of H₂ evolution is proposed to follow an ECEC sequence, where E and C correspond to one-electron reductions and protonations, respectively. On the basis of their values for its p*K_a* and redox potentials, the room temperature values of Δ*G_H*⁺ and Δ*G_H*[–] are estimated as respectively as 57 and 79 kcal/mol for [1H]⁺.

Introduction

Two families of hydrogenases, the [FeFe]-hydrogenases and the [NiFe]-hydrogenases,^{1–4} have stimulated intense work on the development of bioinspired catalysts for hydrogen processing.^{5,6} In the case of the [FeFe]-hydrogenases, the transition from structural to functional model complexes was rapid owing to foundational work conducted, albeit without awareness of the biological connection,⁷ years before the structural characterization of these proteins. Modeling the [NiFe]-hydrogenases has proven more challenging, despite the fact that the relevant proteins had been structurally characterized already in the 1990s. Relative to the [FeFe]-enzymes, the [NiFe]-hydrogenases are

well suited for modeling since these protein are diverse,⁸ sometimes oxygen-tolerant,⁹ and are catalytically biased for H₂ oxidation,¹⁰ which is the more challenging reaction for model complexes.

Diverse structural models for the [NiFe]-hydrogenases have been described,¹¹ including many that feature Ni(SR)₂Fe cores complemented by diatomic ligands on Fe.¹² Unlike model complexes for the active site of the [FeFe]-hydrogenases, where hydrides are numerous, active site models for the [NiFe]-enzymes have until recently lacked hydride ligands.^{13,14} Our contributions to this area of active site modeling have focused

- (1) De Lacey, A. L.; Fernández, V. M.; Rousset, M.; Cammack, R. *Chem. Rev.* **2007**, *107*, 4304–4330.
- (2) Ogata, H.; Lubitz, W.; Higuchi, Y. *Dalton Trans.* **2009**, 7577–7587.
- (3) Fontecilla-Camps, J. C.; Amara, P.; Cavazza, C.; Nicolet, Y.; Volbeda, A. *Nature* **2009**, *460*, 814–822.
- (4) Fontecilla-Camps, J. C.; Volbeda, A.; Cavazza, C.; Nicolet, Y. *Chem. Rev.* **2007**, *107*, 4273–4303.
- (5) Heinekey, D. M. *J. Organomet. Chem.* **2009**, *694*, 2671–2680.
- (6) Gloaguen, F.; Rauchfuss, T. B. *Chem. Soc. Rev.* **2009**, *38*, 100–108.
- (7) Reihlen, H.; von Friedolsheim, A.; Ostwald, W. *Justus Liebigs Ann. Chem.* **1928**, 465, 72–96. Hieber, W.; Spacu, P. *Z. Anorg. Allgem. Chem.* **1937**, *233*, 852–864. King, R. B. *J. Am. Chem. Soc.* **1962**, *84*, 2460. Fauvel, K.; Mathieu, R.; Poilblanc, R. *Inorg. Chem.* **1976**, *15*, 976–978. Winter, A.; Zsolnai, L.; Huttner, G. *Z. Naturforsch.* **1982**, *37b*, 1430–1436.

- (8) Cammack, R.; Frey, M.; Robson, R. *Hydrogen as a Fuel: Learning from Nature*; Taylor & Francis: London, 2001.
- (9) Ludwig, M.; Cracknell, J. A.; Vincent, K. A.; Armstrong, F. A.; Lenz, O. *J. Biol. Chem.* **2009**, *284*, 465–477.
- (10) Vincent, K. A.; Parkin, A.; Armstrong, F. A. *Chem. Rev.* **2007**, *107*, 4366–4413.
- (11) Tard, C.; Pickett, C. J. *Chem. Rev.* **2009**, *109*, 2245–2274. van der Vlugt, J. I.; Meyer, F. *Met. Ions Life Sci.* **2007**, *2*, 181–239.
- (12) Li, Z.; Ohki, Y.; Tatsumi, K. *J. Am. Chem. Soc.* **2005**, *127*, 8950–8951. Ohki, Y.; Yasumura, K.; Kuge, K.; Tanino, S.; Ando, M.; Li, Z.; Tatsumi, K. *Proc. Natl. Acad. Sci. U.S.A.* **2008**, *105*, 7652–7657. Pal, S.; Ohki, Y.; Yoshikawa, T.; Kuge, K.; Tatsumi, K. *Chem. Asian J.* **2009**, *4*, 961–968.
- (13) Mealli, C.; Rauchfuss, T. B. *Angew. Chem., Int. Ed.* **2007**, *46*, 8942–8944.
- (14) Barton, B. E.; Whaley, C. M.; Rauchfuss, T. B.; Gray, D. L. *J. Am. Chem. Soc.* **2009**, *132*, 6942–6943.

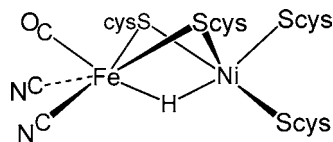


Figure 1. Structure of the active site of the [NiFe]-hydrogenases.

on developing strategies for installing hydride ligands. For example, one could attach Ni modules to substitutionally labile iron hydrides and, complementarily, attach Fe species to Ni hydrides. We have investigated the former route with partial success. The species $[\text{HFe}(\text{CN})_2(\text{CO})_3]^-$, which contains a biomimetic ferrous $[\text{HFe}(\text{CO})(\text{CN})_2]^-$ module, has been prepared efficiently.¹⁵ Although $[\text{HFe}(\text{CN})_2(\text{CO})_3]^-$ undergoes well-behaved substitution reactions, it has not yet been condensed with nickel thiolates. Alternatively, we envisioned reactions of preformed $\text{Ni}(\text{SR})_2\text{Fe}$ ensembles with the equivalent of H^- or H^+ . Hydrides can be installed on diferrous dithiolates using BH_4^- salts.¹⁶ We have generated impure samples of $[(\text{dppe})\text{Ni}(\mu\text{-pdt})(\mu\text{-H})\text{Fe}(\text{CO})(\text{dppe})]^+$ from $[(\text{dppe})\text{Ni}(\mu\text{-pdt})\text{Fe}(\text{CO})_2(\text{dppe})]^{2+}$ via this method ($\text{dppe} = 1,2\text{-bis}(\text{diphenylphosphino})\text{ethane}$, $\text{pdt} = 1,3\text{-propanedithiolate}$).¹⁴

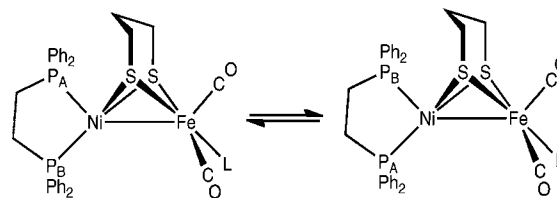
The final approach to nickel–iron hydrides calls for protonation of reduced $\text{Ni}(\text{SR})_2\text{Fe}$ species, a route that is well developed in the modeling of the [FeFe]-hydrogenases.¹⁷ Most structural models feature $\text{Ni}^{\text{II}}(\text{SR})_2\text{Fe}^{\text{II}}$ cores, but a few consist of $\text{L}_2(\text{RS})\text{Ni}^{\text{II}}(\text{SR})\text{Fe}^0(\text{CO})_4$ centers, which in principle could be protonated at iron.¹⁸ Despite its reputed instability, the $\text{Ni}^{\text{I}}(\text{SR})_2\text{Fe}^{\text{I}}$ species $(\text{dppe})\text{Ni}(\mu\text{-pdt})\text{Fe}(\text{CO})_3$ (**1**) was attractive to us.¹⁹ We found that protonation of **1** efficiently affords $[(\text{dppe})\text{Ni}(\mu\text{-pdt})(\mu\text{-H})\text{Fe}(\text{CO})_3]^+$ ($[\text{1H}]^+$), the first hydride-containing model for the [NiFe]-hydrogenases. This heterobimetallic hydride resembles the active site with respect to the presence of a $\text{L}_2\text{Ni}(\text{H})(\text{SR})_2\text{Fe}(\text{CO})\text{L}_2$ core (Figure 1), although it diverges from the biological structure in other ways. The finding that $[\text{1H}]^+$ is an active catalyst for proton reduction demonstrated that even approximate models could prove functional, a finding that underscores the importance of hydride ligands in modeling of the hydrogenases.¹³ In this paper, we describe progress in modifying the $\text{Fe}(\text{CO})_3$ subsite and the chemical consequences thereof. The resulting derivatives are amenable to analysis of design features, including stereodynamics, basicity, and proton relay.

Results

NiFe(pdt)(dppe)(CO)₃ and Hydride Derivatives. Complex **1** has been characterized crystallographically by Schröder et al.¹⁹ The physical properties of our samples differ from those previously reported however.¹⁹ The $^{31}\text{P}\{^1\text{H}\}$ NMR spectrum consists of a broadened singlet at room temperature that decoalesces into two doublets at -68 °C. This pattern is

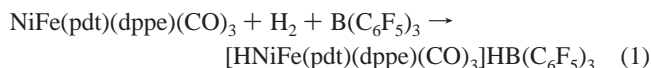
- (15) Whaley, C. M.; Rauchfuss, T. B.; Wilson, S. R. *Inorg. Chem.* **2009**, *48*, 4462–4469.
 (16) van der Vlugt, J. I.; Rauchfuss, T. B.; Whaley, C. M.; Wilson, S. R. *J. Am. Chem. Soc.* **2005**, *127*, 16012–16013.
 (17) Koper, M. T. M.; Bouwman, E. *Angew. Chem., Int. Ed.* **2010**, *49*, 3723–3725.
 (18) Lai, C.-H.; Reibenspies, J. H.; Darensbourg, M. Y. *Angew. Chem., Int. Ed. Engl.* **1996**, *35*, 2390–2393. Verhagen, J. A. W.; Lutz, M.; Spek, A. L.; Bouwman, E. *Eur. J. Inorg. Chem.* **2003**, *2003*, 3968–3974.
 (19) Zhu, W.; Marr, A. C.; Wang, Q.; Neese, F.; Spencer, D. J. E.; Blake, A. J.; Cooke, P. A.; Wilson, C.; Schröder, M. *Proc. Natl. Acad. Sci.* **2005**, *102*, 18280–18285.

Scheme 1. Proposed Ni-Centered Dynamics for **1** ($\text{L} = \text{CO}$), **2** ($\text{L} = \text{P}(\text{OPh})_3$), **3** ($\text{L} = \text{PPh}_3$), and **4** ($\text{L} = \text{PPh}_2\text{py}$)

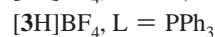
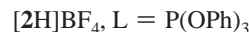
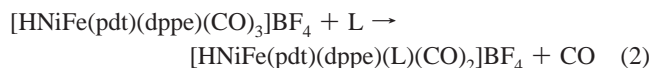


consistent with rotation of the trigonal bipyramidal $\text{Ni}(\text{dppe})$ site (Scheme 1).

Treatment of a CH_2Cl_2 solution of **1** with $\text{HBF}_4 \cdot \text{Et}_2\text{O}$ or $\text{CF}_3\text{CO}_2\text{H}$ resulted in immediate protonation to yield the respective salt of the cationic hydride. The tetrafluoroborate salt ($[\text{1H}]\text{BF}_4$) was isolated as a stable red microcrystalline solid that is soluble in CH_2Cl_2 , THF, MeCN, and MeOH. Its $^{31}\text{P}\{^1\text{H}\}$ NMR spectrum displays a sharp singlet at δ 71. In the ^1H NMR spectrum, the hydride signal appears as a triplet of triplets ($J = 6, 0.6$ Hz, Figure 2). The 6 Hz coupling is a typical J_{PH} for nickel phosphine hydrides, for example, $[\text{HNi}(\text{dppe})_2]\text{AlCl}_4$.²⁰ The smaller coupling, confirmed by the $\{^1\text{H}-^1\text{H}\}$ COSY spectrum, arises from coupling to protons on the dithiolate. The same cationic hydride can be generated from H_2 in the presence of the borane $\text{B}(\text{C}_6\text{F}_5)_3$ ²¹ (eq 1).



Monosubstituted complexes $[\text{HNiFe}(\text{pdt})(\text{dppe})(\text{PR}_3)(\text{CO})_2]\text{BF}_4$ were prepared via thermal and photochemical substitution of $[\text{1H}]\text{BF}_4$ (eq 2).



FT-IR spectra of these adducts feature a pair of comparably intense ν_{CO} bands at about 2025 and 1970 cm^{-1} (Figure 3). The positions of these bands indicate the expected sequence of basicity, that is, $\text{P}(\text{OPh})_3 < \text{PPh}_2\text{Py} < \text{PPh}_3$. The ^1H NMR spectra exhibit doublet of triplets ($J_{\text{PH}} = 35, 4$ Hz) in the hydride region, the coupling to the dppe ligands being slightly less than that of the tricarbonyl hydride, $[\text{1H}]\text{BF}_4$. In addition, all three monosubstituted hydrides displayed an additional doublet of triplets ($J_{\text{PH}} \approx 40, 5$ Hz) accounting for $\sim 1\%$ of the sample (see Figure

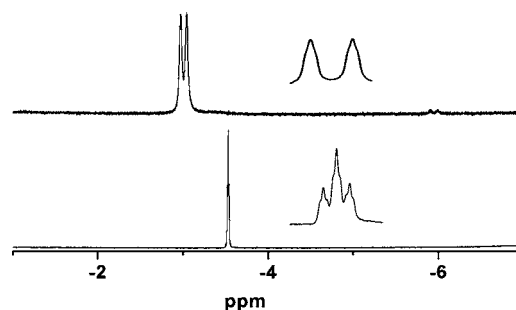


Figure 2. ^1H NMR spectra (500 MHz, CD_2Cl_2 solution) of $[\text{1H}]\text{BF}_4$ (bottom, triplet, $J_{\text{PH}} = 6$ Hz) and of $[\text{3H}]\text{BF}_4$ (top, doublet of triplets, $J_{\text{PH}} = 35$ Hz).

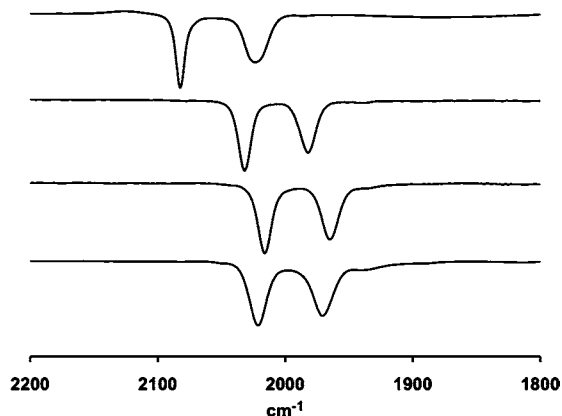


Figure 3. FT-IR spectra in the ν_{CO} region for CH_2Cl_2 solutions of the nickel–iron hydride complexes described in this work (top to bottom): $[\text{1H}]\text{BF}_4$; $[\text{2H}]\text{BF}_4$; $[\text{3H}]\text{BF}_4$; $[\text{4H}]\text{BF}_4$. The ν_{CO} band for the Ni–R state occurs at 1936–1948 cm^{-1} , depending on the organism.¹

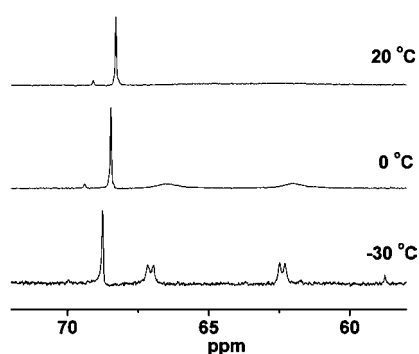


Figure 4. $^{31}\text{P}\{^1\text{H}\}$ NMR (161 MHz) spectra of CD_2Cl_2 solutions of $[\text{3H}]\text{BF}_4$ recorded at various temperatures. The signal at δ 68 is assigned to the $\text{Fe}(\text{PPh}_3)$ center. The dynamic AB quartet at δ 65 is assigned to the Ni(dppe) center. Weak signals near δ 59 and 70 arise from trace impurities of $\text{Ni}(\text{pdt})(\text{dppe})$ and $[\text{HNiFe}(\text{pdt})(\text{dppe})(\text{CO})_3]^+$, respectively.

2). The identity of this second species is unknown, but we suggest that it is an isomer. Such a species is observed in the spectra for $[\text{2H}]^+$, $[\text{3H}]^+$, and $[\text{4H}]^+$, but its NMR shift varies with the identity of the phosphorus ligand.

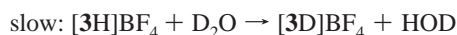
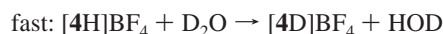
Variable temperature $^{31}\text{P}\{^1\text{H}\}$ NMR spectra provide insights into the dynamics that cannot be readily analyzed for the more symmetrical $[\text{1H}]\text{BF}_4$. The signal assigned to dppe (δ 65) was broad at room temperature but decoalesced at -60 °C into two doublets. The singlet for PPh_3 remained unchanged throughout this experiment (Figure 4). This DNMR pattern is consistent with both a rocking of the $\text{Fe}(\text{PPh}_3)(\text{CO})_2$ subunit between two equivalent structures (Scheme 2) and rotation of the Ni(dppe) center. We have previously shown that related diiron dithiolates, for example, compounds such as $\text{Fe}_2(\text{pdt})(\text{CO})_4(\text{diphosphine})$, are stereochemically nonrigid.²² Variable temperature ^{13}C NMR spectra show that the $\text{PCH}_2\text{CH}_2\text{P}$ signals ($\Delta\nu = 180$ Hz at -60 °C)

are fully coalesced at $+19$ °C, but the SCH_2 signals ($\Delta\nu = 91$ Hz at -30 °C) remain completely distinct. The finding that more closely spaced SCH_2 signals must coalesce at higher temperatures than the $\text{PCH}_2\text{CH}_2\text{P}$ signals indicates that the rocking of the $\text{Fe}(\text{CO})_2\text{PPh}_3$ group is a higher energy process and rotation of the Ni(dppe) center proceeds with a lower barrier.

Complex $[\text{3H}]\text{BF}_4$ was further characterized by X-ray crystallography, which confirmed that PPh_3 is *cis* to the hydride (Figure 5). The $\text{Fe}(1)\text{--Ni}(1)$ distance of 2.6432(7) Å is only slightly longer than that of $[\text{1H}]\text{BF}_4$ (2.6131(14) Å). The Fe–Ni distance in the *D. vulgaris* enzyme for the Ni–C/Ni–R state is 2.55 Å.² The bridging hydride position for $[\text{3H}]\text{BF}_4$ is unsymmetrical, being closer to iron than nickel by 0.40 Å, whereas in $[\text{1H}]\text{BF}_4$ the hydride ligand is closer to iron by only 0.18 Å. The unsymmetrical character of the hydride ligand is also indicated by the diminished value of J_{PH} between the hydride and the dppe ligand (4 Hz vs 35 Hz for coupling to PPh_3). The $\text{Fe}(1)\text{--S}(1)\text{--Ni}(1)$ angle in $[\text{3H}]\text{BF}_4$ (71.42(3)°) is almost identical to that for $[\text{1H}]\text{BF}_4$ (70.39(6)°). The OC–Fe–CO angle is 99°, vs the value of 96° calculated from the difference in the intensities of the two ν_{CO} bands.²³

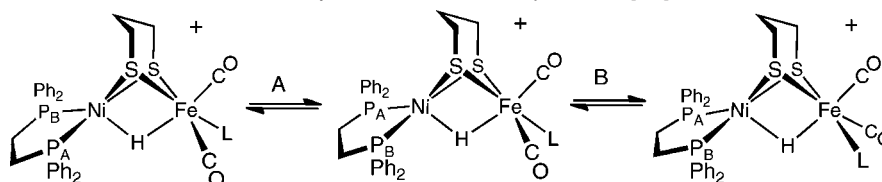
$\text{NiFe}(\text{pdt})(\text{dppe})(\text{PPh}_3)(\text{CO})_2$ (**3**) can be prepared in analytical purity by the deprotonation of $[\text{3H}]\text{BF}_4$ with NaOMe. The ν_{CO} bands of **3** (CH_2Cl_2 : 1971, 1916 cm^{-1}) shift by about 45 cm^{-1} toward lower energy. The $^{31}\text{P}\{^1\text{H}\}$ NMR spectrum (Figure 6) of a CD_2Cl_2 solution at room temperature displays a triplet (δ 55) assigned to the PPh_3 ligand and two broad signals for the dppe (δ 77, 45). Upon cooling the sample to -20 °C, the dppe signals sharpen to the expected AB quartet and the PPh_3 signal appears as a doublet-of-doublets. This dynamic behavior is analogous to that proposed for **1**.

The pyridylphosphine hydride $[\text{4H}]^+$ displays more complexity than $[\text{2H}]^+$ and $[\text{3H}]^+$. Addition of D_2O to a d_6 -acetone solution of $[\text{4H}]\text{BF}_4$ in CD_2Cl_2 solution resulted in conversion to $[\text{4D}]\text{BF}_4$ within seconds. Under the same conditions, the corresponding PPh_3 derivative $[\text{3H}]\text{BF}_4$ was found to exchange only slowly ($t_{1/2} = 20$ min). Similarly, $[\text{4H}]\text{BF}_4$ was rapidly deprotonated by NEt_3 , whereas deprotonation of the analogous PPh_3 derivative required hours under comparable conditions.



The IR spectrum of $[\text{4H}]\text{BF}_4$ is more complex than that for $[\text{2H}]\text{BF}_4$ and is indicative of a mixture of three equilibrating species. In THF solution, bands are observed not only for the expected cationic hydride $[\text{4H}]^+$, but also for neutral **4** and the N-protonated hydride $[\text{4H}_2]^{2+}$. At room temperature, the relative

Scheme 2. Representation of the Fe- and Ni-Centered Dynamic Processes Proposed for $[\text{2H}]\text{BF}_4$



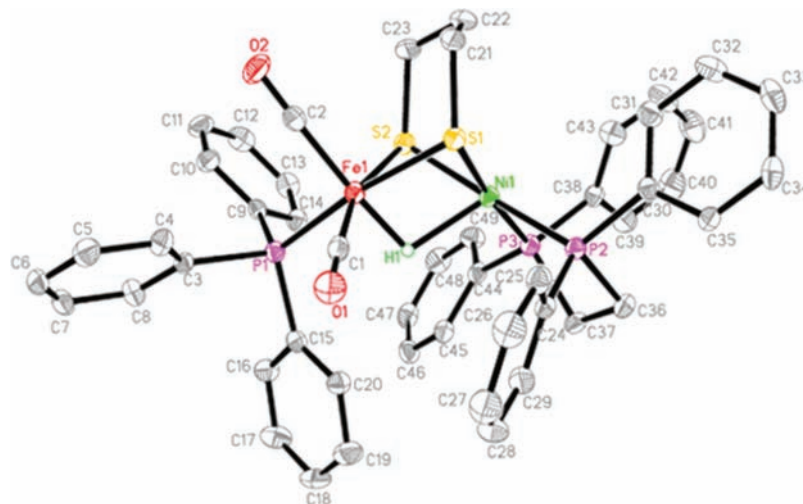


Figure 5. Structure of $[3H]BF_4$. Selected distances (Å): Fe(1)–Ni(1), 2.6432(7); Fe(1)–H(1), 1.49(3); Ni(1)–H(1), 1.89(3). Selected Bond angles (deg): S(2)–Fe(1)–S(1), 83.27(4); S(2)–Fe(1)–P(1), 93.58(4); C(1)–Fe(1)–C(2), 99.93(17).

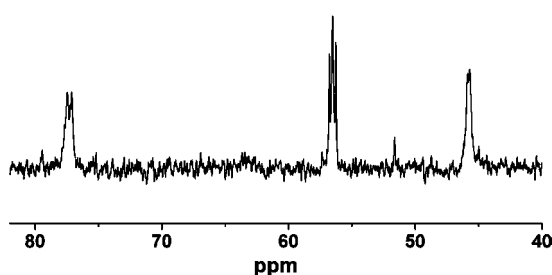
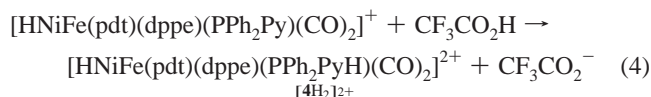


Figure 6. $^{31}P\{^1H\}$ NMR spectrum (161 MHz, CD_2Cl_2 , 20 °C) of **3**. Signals at δ 77 and 45 are assigned to dppf, the signal at δ 55 is assigned to PPh_3 .

amounts of the organometallic components in the solution were estimated by simulation of the IR spectrum, giving K_{prot} (eq 3).

$$K_{prot} = \frac{[4]}{[4H_2^{2+}][4H^+]} \approx 0.03 \quad (3)$$

Addition of excess CF_3CO_2H to a CH_2Cl_2 solution of $[4H]^+$ gave a new hydride with a concomitant increase of ν_{CO} by 10 cm^{-1} . This shift is consistent with protonation of the pyridine ligand giving $[4H_2]^{2+}$ (eq 4). The 1H NMR spectrum of $[4H_2]^{2+}$ features a doublet of triplets centered at $\delta = -3.11$ ($J_{PH} = 40$, 3.5 Hz). The $^{31}P\{^1H\}$ NMR spectrum resembles that for $[3H]BF_4$. Consistent with the weak donor ability of PPh_2PyH^+ , $[4H_2]^{2+}$ is not stable for prolonged periods and degrades to $[1H]^+$ and free phosphine.



Redox Properties and Catalytic Hydrogen Evolution. Cyclic voltammetry indicates that the complexes $[1H]BF_4$, $[2H]BF_4$,

Table 1. Selected Electrochemical Properties of Nickel–Iron Hydrides^a

| complex | $E_{1/2}$ (V) vs $Fe^{0/+}$ | i_{pa}/i_{pc} (at 0.1 V/s) |
|---------------|-----------------------------|------------------------------|
| $[1H]^+$ | −1.29 | 0.26 |
| $[2H]^+$ | −1.44 | 0.93 |
| $[3H]^+$ | −1.49 | 0.06 |
| $[4H]^+$ | −1.49 | 0.00 |
| $[4H_2]^{2+}$ | −1.28 | – |

^a Data were collected on 1 mM freshly prepared MeCN solution of nickel–iron hydride and 0.1 M $[NBu_4]PF_6$ as electrolyte.

and $[3H]BF_4$, undergo at least quasi-reversible reductions at about −1.5 V (Table 1). The corresponding reduction for $[4H]BF_4$ was irreversible. For complex $[2H]BF_4$, this couple was partially reversible with i_{pa}/i_{pc} of 0.93. The one-electron nature of the reduction of $[2H]^+$ is indicated by the separation of the peak potentials of $\Delta E_p \approx 65$ mV. Additionally, the scan rate dependence for the $[2H]^{+/0}$ and $[2]^{0/+}$ couples are very similar. We have independently established the one-electron nature of the oxidation of **2** to give the mixed-valence $Ni^I Fe^I$ complex (Figure 7).²⁴ The oxidation of CH_2Cl_2 solutions of $[2H]BF_4$, $[3H]BF_4$, and $[4H]BF_4$ occur near 0.5 V vs $Fe^{0/+}$ and are irreversible.

Upon addition of CF_3CO_2H ($pK_a^{MeCN} = 12.65$,²⁵ $E^0 = -0.89$ V)²⁶ to CH_2Cl_2 solutions of $[2H]^+$ and $[3H]^+$, cyclic voltammograms displayed increased cathodic current coinciding with the hydride reduction event indicative of proton reduction catalysis (Figure 9). At the relevant potentials (−1.5 V) proton reduction by the glassy carbon working electrode was confirmed to be negligible.²⁶ In the case of $[4H]^+$, addition of CF_3CO_2H resulted in the appearance of a new catalytic current about 200 mV milder than the $[4H]^{+/0}$ couple (Figure 10). We attribute this new feature to catalysis by the *N*-protonated pyridine $[4H_2]^{2+}$ complex, consistent with the previous spectroscopic results. Because $[4H_2]^{2+}$ degrades into $[1H]^+$ at high concentrations of CF_3CO_2H (10–100 equiv), the voltammograms display an additional catalytic wave for $[1H]^+$.

- (20) Schunn, R. A. *Inorg. Chem.* **1970**, *9*, 394–395.
 (21) Stephan, D. W. *Dalton Trans.* **2009**, *312*, 9–3136. Heiden, Z. M.; Zampella, G.; De Gioia, L.; Rauchfuss, T. B. *Angew. Chem., Int. Ed.* **2008**, *47*, 9756–9759.
 (22) Justice, A. K.; Zampella, G.; De Gioia, L.; Rauchfuss, T. B.; van der Vlugt, J. I.; Wilson, S. R. *Inorg. Chem.* **2007**, *46*, 1655–1664. Justice, A. K. Ph.D. Thesis, University of Illinois at Urbana-Champaign, 2008.
 (23) Braterman, P. S. *Metal Carbonyl Spectra*; Academic Press: London, 1975.

- (24) Schilter, D.; Rauchfuss, T. B. Unpublished results.
 (25) Izutsu, K. *Acid-Base Dissociation Constants in Dipolar Aprotic Solvents*; Blackwell Scientific Publications: Oxford, U.K., 1990.
 (26) Felton, G. A. N.; Glass, R. S.; Lichtenberger, D. L.; Evans, D. H. *Inorg. Chem.* **2006**, *45*, 9181–9184.

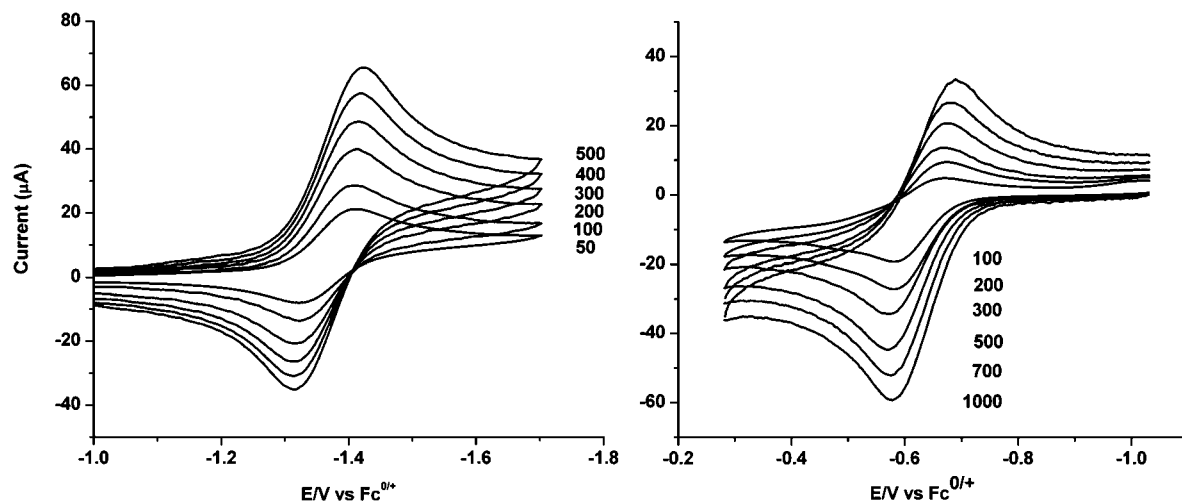


Figure 7. Cyclic voltammograms of a 1.85 mM MeCN solution of $[2H]^+$ (left) and a 1.68 mM 9:1 MeCN/ CH_2Cl_2 solution (0.1 M $[NBu_4]PF_6$) of **2** (right) at various scan rates, denoted in mV/s.

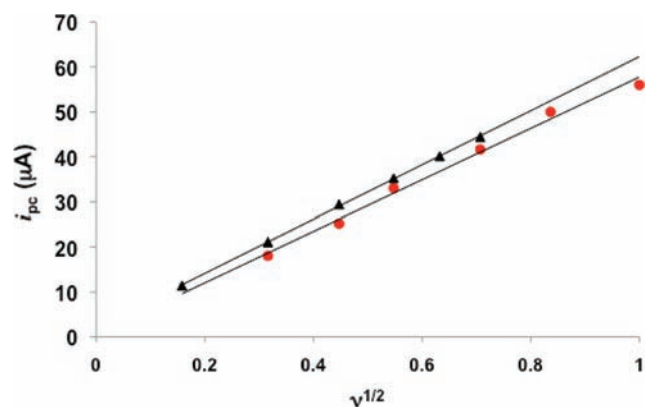


Figure 8. Scan rate dependence of i_{pc} for the couples $[2H]^+/0$ and $2^{0/+}$ in CH_2Cl_2 solution (1.8 mM complex, 0.1 M $[NBu_4]PF_6$).

Plots of i_c/i_p (i_c = catalytic current, i_p = peak current in the absence of acid) vs $[CF_3CO_2H]$ are linear up to about $i_c/i_p = 16$ – 20 (Figure 11). This linear dependence indicates that H_2 evolution follows protonation of the reduced hydride, that is, the rate is second order in $[H^+]$.²⁷ The initial slope of this plot

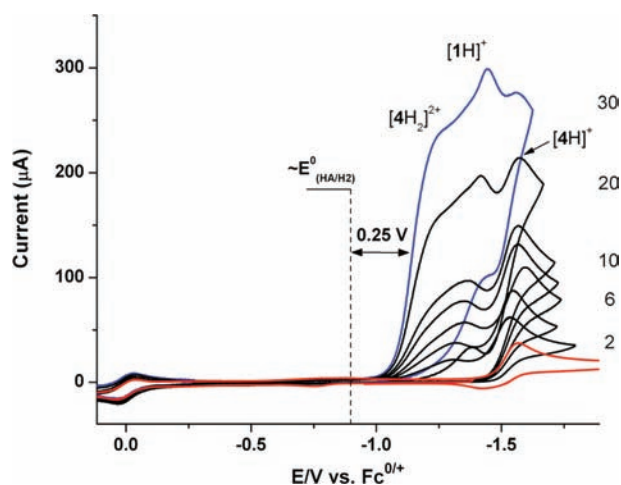


Figure 10. Cyclic voltammograms of a CH_2Cl_2 solution (0.74 mM) of $[4H]BF_4$ with increasing equiv of CF_3CO_2H (denoted on right). Conditions: see Figure 9.

is a measure of the acid-dependent rate-determining step. For the hydrides investigated, this step is the protonation of

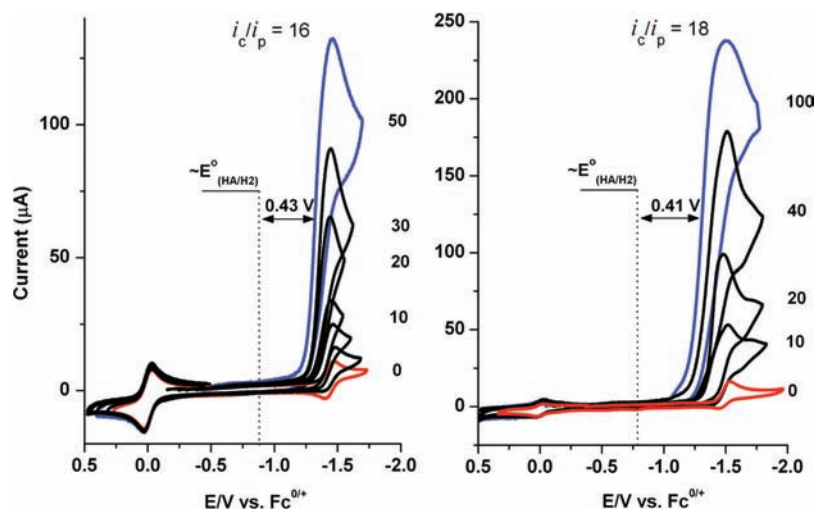


Figure 9. Cyclic voltammograms of $[2H]BF_4$ (left) and $[3H]BF_4$ (right) with increasing equiv of CF_3CO_2H (denoted on right). Overpotentials were estimated by the standard potential for hydrogen evolution from CF_3CO_2H in MeCN solution. Conditions: ~ 0.5 mM in CH_2Cl_2 (see experimental), 0.1 M $[NBu_4]PF_6$, scan rate 0.1 V/s, glassy carbon working electrode ($d = 3.0$ mm); Ag wire pseudoreference with internal Fc standard at 0 V; Pt counter electrode.

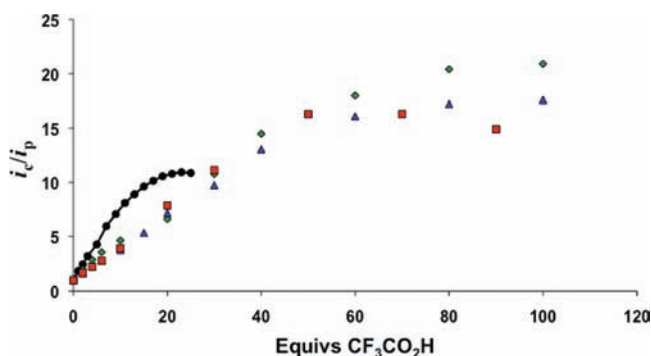


Figure 11. Influence of [acid]–catalyst ratio on catalytic current (i_c/i_p) for $[1H]BF_4$ (black circles), $[2H]BF_4$ (red squares), $[3H]BF_4$ (blue triangles), and $[4H]BF_4$ (green diamonds). Conditions: see Figure 9.

Ni(I)Fe(I) precursors to form hydrides. Catalysis by the sterically more accessible tricarbonyl **1** displays a steeper initial slope than the substituted derivatives **2** and **3** even though the latter are more basic. Relative to **2** and **3**, the greater steric accessibility of **1** toward protonation is consistent with the finding that $[1H]^+$ is rapidly deprotonated by Et_3N whereas $[3H]^+$ requires hours to deprotonate by the same strong base. The relative catalytic activity can be estimated from the acid-independent regions of the graph of i_c/i_p vs $[CF_3CO_2H]$.²⁸ The values for $i_c/i_p = 16$ – 20 , indicating an acid-independent rate constant between 50 – $75\ s^{-1}$. For the tricarbonyl $[1H]^+$, the i_c/i_p of 10 corresponds to an acid-independent rate constant of $20\ s^{-1}$.

To determine overpotential, electrocatalysis was conducted in MeCN solution, where the standard reduction potential of the acid to release H_2 , E^0_{HA/H_2} , has been determined.²⁹ For CF_3CO_2H in MeCN solution, E^0 is $-0.89\ V$. Cyclic voltammetry of a freshly prepared MeCN solution of $[3H]^+$ displayed the $[3H]^{+/0}$ couple at $-1.45\ V$, and the cathodic current dramatically increased upon addition of CF_3CO_2H . The overpotential is estimated at $430\ mV$ (Figure 9). For the pyridinium complex $[4H_2]^{2+}$, overpotential is significantly smaller, $\sim 260\ mV$ (Figure 10).

Relevant to the mechanism of H_2 production is the finding that the reversibility of the $[2H]^{+/0}$ couple is diminished in the presence of $[HNET_3]BF_4$. This effect is consistent with the reduced derivative $[2H]^0$ being sufficiently basic to undergo protonation by $[HNET_3]^+$. Since $[HNET_3]BF_4$ is unable to protonate **2**, the system $2/[HNET_3]^+$ is catalytically inactive (in contrast to $2/[CF_3CO_2H]^+$). To further clarify the mechanism of hydrogen production, we found that in the presence of excess acid, the catalytic current depends linearly on the concentration of $[3H]^+$. Thus, the catalysis is first-order in $[3H]^+$.

Acidity of Nickel–Iron Hydrides. To better understand the thermodynamic properties of the catalysts, we sought to determine both the pK_a 's of the new nickel–iron hydrides and the electrochemical properties of their conjugate bases. Compounds **1** and **2** are poorly soluble in MeCN, a solvent with a well-established pK_a scale,³⁰ We instead employed PhCN as the solvent for the pK_a determinations. Although PhCN does

Table 2. Thermodynamic Data (E 's in V vs $Fc^{0/+}$, ΔG 's in kcal/mol at 298 K for MeCN Solutions, NiFe = NiFe(pdt)(dppe)L(CO)₂ ($T = 298\ K$)

| | pK_a | $E(NiFe^{0/+})$ | $E(NiFe^{+/2+})$ | $E(HNiFe^{+/0})$ | $\Delta G_{H\cdot}$ | ΔG_H |
|----------|--------|-----------------|------------------|------------------|---------------------|--------------|
| $[1H]^+$ | 10.7 | -0.543 | -0.124 | -1.29 | 57 | 79 |
| $[3H]^+$ | 14.9 | -0.722 | -0.191 | -1.49 | 58 | 79 |

not have an established pK_a scale, others have found that it behaves similarly to MeCN solutions.²⁸ A dilute solution of $[1H]^+$ in PhCN with one equiv of aniline ($[PhNH_3]BF_4$, $pK_a^{MeCN} = 10.7$) afforded a 1:1 equilibrium mixture of $[1H]^+$ and **1**, indicating a pK_a of 10.7 for $[1H]^+$. Similarly, four equiv of 4-methoxypyridine ($[4\text{-methoxypyridinium}]BF_4$, $pK_a^{MeCN} = 14.23$)³⁰ and $[3H]^+$ provided a 2:1 equilibrium ratio of **3** and $[3H]^+$, as determined by ^{31}P NMR spectroscopy. Although the organometallic species decomposes over the course of several hours, we assign the pK_a as 14.9 ± 0.1 as the **3**: $[3H]^+$ ratio remained unchanged throughout the decomposition. For comparison with these results, the μ -hydrido diiron complex $[HFe_2(pdt)(CO)_4(PMe_3)_2]BF_4$ has pK_a^{MeCN} of 12.³¹

Using cyclic voltammetry, we determined the oxidation potentials of **1** and **3**. Similar to the pK_a determination, PhCN was used to approximate $E_{1/2}$ values on the MeCN scale. A 1 mM solution of **1** in PhCN displayed two oxidation events, one reversible at $-0.543\ V$ and a second irreversible event at $-0.124\ V$ (Table 2). The cyclic voltammogram for **3** was similar, displaying a reversible oxidation at $-0.722\ V$ and an irreversible oxidation event at $-0.191\ V$. We assign these couples as one-electron processes. The oxidation of **1** with one equiv of ferrocenium has been shown to afford the monocation.¹⁴

Discussion

The new hydride complexes are confirmed to be robust and functional models for the [NiFe]-hydrogenases, at least with respect to certain structural features and their ability to catalyze hydrogen evolution. Specifically, the hydrides represent structural mimics of the Ni–R form of these enzymes, an $S = 0$ state that is thought to feature an $Fe(\mu\text{-SR})_2(\mu\text{-H})Ni$ core.¹ In the model complexes, the coordination sphere at Ni is square pyramidal, having rearranged from the tetrahedral geometry of the Fe(I)Ni(I) precursor. Such a rearrangement is unlikely in the protein, wherein the Ni center adopts a geometry intermediate between square-planar and tetrahedral.⁴

The present paper describes examples of hydride complexes that sustain at least quasi-reversible redox events. Reversible redox has been observed in a few bimetallic hydrides³² but is rare for monometallic hydrides where redox changes the pK_a by many orders of magnitude, which often precludes reversibility.^{33,34} Nature's selection of bimetallic active sites in the [FeFe]- and [NiFe]-hydrogenases thus provides a way to soften the effect of redox on the acid–base properties of the hydride. The pK_a and electrochemical data allow us to estimate the homolytic and heterolytic bond energies for the bond between the NiFe center and the $\mu\text{-H}$ ligand. Following the relations in eq 5 and 6, the free energy of $H\cdot$ donation, $\Delta G_{H\cdot}$, is calculated to be $57\ kcal/mol$. These values indicate relatively weak M–H bonds,^{34,35}

(27) Wilson, A. D.; Newell, R. H.; McNevin, M. J.; Muckerman, J. T.; Rakowski DuBois, M.; DuBois, D. L. *J. Am. Chem. Soc.* **2006**, *128*, 358–366.

(28) Frazee, K.; Wilson, A. D.; Appel, A. M.; Rakowski DuBois, M.; DuBois, D. L. *Organometallics* **2007**, *26*, 3918–3924.

(29) Wayner, D. D. M.; Parker, V. D. *Acc. Chem. Res.* **2002**, *26*, 287–294.

(30) Kaljurand, I.; Kütt, A.; Sooväli, L.; Rodima, T.; Mäemets, V.; Leito, I.; Koppel, I. A. *J. Org. Chem.* **2005**, *70*, 1019–1028.

(31) Eilers, G.; Schwartz, L.; Stein, M.; Zampella, G.; de Gioia, L.; Ott, S.; Lomoth, R. *Chem.–Eur. J.* **2007**, *13*, 7075–7084.

(32) Barton, B. E.; Rauchfuss, T. B. *Inorg. Chem.* **2008**, *47*, 2261–2263.

(33) Tilset, M. *J. Am. Chem. Soc.* **1992**, *114*, 2740–2741. Cheng, T.-Y.; Szalda, D. J.; Zhang, J.; Bullock, R. M. *Inorg. Chem.* **2006**, *45*, 4712–4720. Hamon, P.; Toupet, L.; Hamon, J.-R.; Lapinte, C. *Organometallics* **1992**, *11*, 1429–1431.

Table 3. Fe–H and Ni–H Bond Distance (Å) in Diiron and Nickel–Iron Dithiolato Hydrides

| hydride | M–H distances | $\Delta d(\text{M–H})$ |
|---|---|------------------------|
| $[\text{HFe}_2(\text{pdt})(\text{CO})_4(\text{dppe})]\text{BF}_4^{37}$ | (dppe) ^{dibasal} (CO)Fe–H: 1.627(3) (CO) ₃ Fe–H: 1.640(4) | 0.013 |
| $[\text{HFe}_2(\text{pdt})(\text{CO})_4(\text{NHC-chelate})]\text{BF}_4^{38}$ | (NHC) ₂ (CO)Fe–H: 1.710 (CO) ₃ Fe–H: 1.562 Å | 0.15 |
| <i>unsym</i> - $[\text{HFe}_2(\text{SC}_2\text{H}_4\text{PMe}_2)_2(\text{CO})_4]\text{BF}_4^{39}$ | (PR ₃) ^{apical} (CO) ₂ Fe–H: 1.59(1) (PR ₃) ^{basal} (CO) ₂ Fe–H: 1.74(1) | 0.15 |
| <i>cis</i> - $[\text{HFe}_2(\text{pdt})(\text{CN})(\text{CO})_4(\text{PMe}_3)]\text{BF}_4^{40}$ | (PMe ₃) ^{basal} (CO) ₂ Fe–H: 1.63(1) (NC) ^{basal} (CO) ₂ Fe–H: 1.70(1) | 0.07 |
| $[\text{HNiFe}(\text{pdt})(\text{dppe})(\text{CO})_3]\text{BF}_4^{14}$ | Fe–H: 1.46(6) Ni–H: 1.64(6) | 0.18 |
| $[\text{HNiFe}(\text{pdt})(\text{dppe})(\text{PPh}_3)(\text{CO})_2]\text{BF}_4$ | Fe–H: 1.49(3) Ni–H: 1.89(3) | 0.4 |

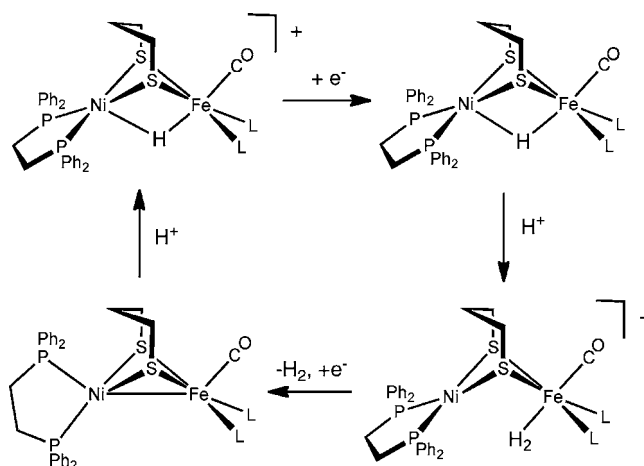
consistent with the stability of the mixed valence cations. Substitution of CO by PPh₃ affects the [NiFe]^{I,I,II} and [NiFe]^{I,II,II} couples as well as the pK_a. Comparing [1H]⁺ to [3H]⁺, the ΔpK_a of 4.2 corresponds to 5.7 kcal/mol. The $\Delta E_{1/2}$ of the [HNiFe]⁺⁰ couples corresponds to 4.6 kcal/mol. Consequently, although [3H]⁺ is more difficult to reduce than [1H]⁺, its formation requires weaker acids and thus its catalytic function operates at a lower overpotential.

Although the 1^{0/+} and 3^{0/+} couples are reversible, the couples 1⁺²⁺ and 3⁺²⁺ are not. Both are required to calculate ΔG_{H} , which is related to the affinities of [1]²⁺ and [3]²⁺ for H[−]. The ~0.5 V difference observed between the first and second potentials is expected,³⁶ so these redox potentials were used to approximate the hydride donor strength for [1H]⁺ and [3H]⁺ (Table 2). These data suggest that the [1]²⁺ and [3]²⁺ have very high affinities for hydrides, the high positive charge and bimetallic structure being contributing factors.

$$\Delta G_{\text{H}^+} = 1.37pK_a + 23.06E_{1/2}^{\text{I,I,II}} + 54.9 \quad (5)$$

$$\Delta G_{\text{H}^-} = 1.37pK_a + 23.06E_{1/2}^{\text{I,I,II}} + 23.06E_{1/2}^{\text{I,II,II}} + 79.6 \quad (6)$$

One of the more striking results is the asymmetry of the Fe–H–Ni linkage, which we propose is relevant to the mechanism by which these complexes reduce protons. In the parent hydride [HNiFe(pdt)(dppe)(CO)₃]₂BF₄, ([1H]BF₄) the difference of the iron-hydride and nickel-hydride bond distances ($\Delta d(\text{M–H})$) is 0.15 Å, whereas in [HNiFe(pdt)(dppe)(PPh₃)(CO)₂]₂BF₄, the Ni–H bond is 0.4 Å longer than the Fe–H bond (Table 3). Although terminal hydrides are invoked for the catalytic mechanism of [FeFe]-hydrogenases, catalytically active μ -hydrido diiron dithiolates have been reported.⁶ The asymmetry of the Ni–H–Fe linkage in the present cases suggests that even

Scheme 3. Catalytic Cycle Proposed for Hydrogen Evolution by [HNiFe(pdt)(dppe)L₂(CO)]BF₄**Table 4.** Estimated Catalytic Properties of the Hydrides. Conditions: see Experimental Section

| catalyst | E_{cat}^a (V, vs Fc ^{0/+}) | rate ^b (s ^{−1}) | overpotential ^c (V) |
|---|---|--------------------------------------|--------------------------------|
| [1H] ⁺ | −1.20 | 20 | 0.31 |
| [2H] ⁺ | −1.32 | 50 | 0.43 |
| [3H] ⁺ | −1.30 | 50 | 0.41 |
| [4H] ⁺ | ~−1.3 | 50 | ~0.4 |
| [4H ₂] ²⁺ | −1.15 | 50 | 0.26 |
| [NiFe]-hydrogenase (<i>A. vinosum</i>) | −0.345 (pH 7.4) ^d | 500 ^e | 0 ⁴⁵ |

^a For [1H]⁺ through [4H]⁺, potential at $i_{\text{pc}}/2$ for an acid-independent voltammogram.²⁶ Potentials can be corrected from Fc⁺⁰ (MeCN) to NHE using the relation $E^{\text{NHE}} = E^{\text{Fc}} + 0.717 \text{ V}$.⁴⁶ ^b Estimated from acid-independent region of i_p/i_{pc} vs [acid] plot, see ref 28. ^c Calculated using the relation Overpotential is the difference between E^{cat} and −0.89 V.²⁶ ^d Onset potential, 40 °C, vs NHE.⁴⁷ ^e Lower limit estimate, 30 °C, pH 6.

in the [NiFe] enzymes, the Fe–H bond may be described as having the character of a terminal (vs bridging) hydride.

Catalysis by these complexes is proposed to operate via the sequence of reactions in Scheme 3. The voltammetric responses indicate that the reaction is second order in protons and first order in the bimetallic complex. The rate of protonation depends on both the basicity of the metal center and steric effects.⁴¹ The associated acid-dependent rate constants are not effective benchmarks for catalytic efficiency, in part because they depend on the proton source.⁴² More useful are the relative rates for catalysis in the acid-independent regime obtained at high [H⁺], as well as the overpotential (Table 4).⁴³ This high [H⁺] regime is proposed to resemble enzymatic conditions where protons are efficiently provided to the NiFe center.⁴⁴

- (34) Tilset, M. In *Comprehensive Organometallic Chemistry III*; Crabtree, R. H., Mingos, D. M. P., Eds.; Elsevier: Oxford, 2007; pp 279–305.
- (35) Choi, J.; Pulling, M. E.; Smith, D. M.; Norton, J. R. *J. Am. Chem. Soc.* **2008**, *130*, 4250–4252. Wang, D.; Angelici, R. J. *J. Am. Chem. Soc.* **1996**, *118*, 935–942.
- (36) Houser, E. J.; Venturelli, A.; Rauchfuss, T. B.; Wilson, S. R. *Inorg. Chem.* **1995**, *34*, 6402.

- (37) Ezzaher, S.; Capon, J.-F.; Gloaguen, F.; Pétillon, F. Y.; Schollhammer, P.; Talarmin, J.; Pichon, R.; Kervarec, N. *Inorg. Chem.* **2007**, *46*, 3426–3428.
- (38) Morvan, D.; Capon, J.-F.; Gloaguen, F.; Le Goff, A.; Marchivie, M.; Michaud, F.; Schollhammer, P.; Talarmin, J.; Yaouanc, J.-J. *Organometallics* **2007**, *26*, 2042–2052.
- (39) Zhao, X.; Hsiao, Y.-M.; Lai, C.-H.; Reibenspies, J. H.; Darensbourg, M. Y. *Inorg. Chem.* **2002**, 699–708.
- (40) Gloaguen, F.; Lawrence, J. D.; Rauchfuss, T. B.; Bénard, M.; Rohmer, M.-M. *Inorg. Chem.* **2002**, *41*, 6573–6582.
- (41) Kramarz, K. W.; Norton, J. R. *Prog. Inorg. Chem.* **1994**, *42*, 1–65.
- (42) Ezzaher, S.; Capon, J.-F.; Dumontet, N.; Gloaguen, F.; Pétillon, F. Y.; Schollhammer, P.; Talarmin, J. *J. Electroanal. Chem.* **2009**, *626*, 161–170.
- (43) Rakowski Dubois, M.; Dubois, D. L. *Acc. Chem. Res.* **2009**, *42*, 1974–1982.

Pyridylphosphines confer fascinating properties to certain catalysts⁴⁸ and offered the possibility of facilitating proton transfer.⁴⁹ When installed on diiron dithiolates, pyridyl phosphines undergo *N*-protonation, which leads to milder E_{cat} , an effect attributable to an electrostatic influence.⁵⁰ We observe similar effects in this study: the overpotential decreases by ~ 140 mV for the dication $[\text{4H}_2]^{2+}$ vs $[\text{4H}]^+$ (Table 4). The amine also accelerates the deprotonation of the μ -hydride, which is otherwise slow. The pathway by which this deprotonation occurs is suggested by the observation that the hydride exists in equilibrium with the pyridinium salt. In the protein, the protons exchange between the metal centers (hydride ligands) and the terminal thiolate ligands.⁴

Experimental Section

Unless otherwise indicated, reactions were conducted using Schlenk and cannula-filtration techniques at reduced temperatures. Solvents for syntheses were HPLC-grade and further purified using an alumina filtration system (Glasscontour Co., Irvine, CA), NMR solvents were either dried with CaH_2 and stored under nitrogen over activated molecular sieves or purchased as ampules from Cambridge Isotope Laboratories. Diiron nonacarbonyl, tetrafluoroboric acid in diethyl ether, triphenylphosphite, triphenylphosphine, and trifluoroacetic acid were purchased from Aldrich and used as received. Tetrabutylammonium hexafluorophosphate (Aldrich) was recrystallized from methylene chloride and hexane. NMR spectra were recorded at room temperature on a Varian Mercury spectrometer. NMR chemical shifts are quoted in ppm; spectra are referenced to TMS for ^1H and 85% H_3PO_4 for $^{31}\text{P}\{^1\text{H}\}$ NMR spectra.

NiFe(pdt)(dppe)(CO)₃, 1. To a 500-mL round bottomed Schlenk flask with stir bar was added 2.25 g (4.01 mmol) of Ni(pdt)(dppe), 1.52 g (4.19 mmol) of $\text{Fe}_2(\text{CO})_9$, and 40 mL of CH_2Cl_2 . After stirring the red slurry for 6 h, solvent was removed under vacuum, and the red residue was washed with four 30 mL portions of MeCN to remove $\text{Fe}_2(\text{pdt})(\text{CO})_6$ and $\text{Fe}(\text{CO})_5$. The remaining red-green solid was extracted into ca. 5 mL of CH_2Cl_2 , and this extract was filtered through 4×12 cm plug of silica gel, rinsing with CH_2Cl_2 . A mobile green product eluted, leaving unreacted Ni(pdt)(dppe). The green solution was then concentrated and then diluted with 100 mL of hexane to precipitate green microcrystals. Yield: 0.745 g (1.06 mmol, 27%). ^1H NMR (500 MHz, CD_2Cl_2 , 20 °C): δ 1.3 (1H, *qt*, axial $(\text{SCH}_2)_2\text{CH}_2$), 1.85 (1H, *dt*, equatorial $(\text{SCH}_2)_2\text{CH}_2$), 1.9 (2H, *t*, axial $(\text{SCH}_2)_2\text{CH}_2$), 2.5 (2H, *dt*, equatorial $(\text{SCH}_2)_2\text{CH}_2$), 2.2 (4H, *m*, $\text{PCH}_2\text{CH}_2\text{P}$), 7.4–7.7 (20H, *m*, C_6H_5). $^{31}\text{P}\{^1\text{H}\}$ NMR (202 MHz, CD_2Cl_2): δ 63.6. FT-IR (CH_2Cl_2): $\nu_{\text{CO}} = 2028, 1952 \text{ cm}^{-1}$.

[HNiFe(pdt)(dppe)(CO)₃]BF₄, [1H]BF₄. To a 100-mL round bottomed Schlenk flask with magnetic stir bar was added 1.25 g (1.78 mmol) of **1** and 10 mL of CH_2Cl_2 . To this green solution was added 0.30 mL (2.078 mmol) of $\text{HBF}_4 \cdot \text{Et}_2\text{O}$, immediately producing a red solution. The solution was then concentrated under vacuum and the product was precipitated by the addition of 20 mL

of Et_2O . Recrystallization from $\text{CH}_2\text{Cl}_2/\text{Et}_2\text{O}$ afforded red microcrystals. Yield: 1.35 g (1.71 mmol, 96%). ^1H NMR (500 MHz, CD_2Cl_2 , 20 °C): δ -3.53 (1H, *tt*: $J_{\text{PH}} = 6, J_{\text{HH}} = 0.6$ Hz correlates with signal at $\delta 2.5$, HNiFe), 1.57 (1H, *qt*, axial $(\text{SCH}_2)_2\text{CH}_2$), 2.0 (2H, *t*, axial $(\text{SCH}_2)_2\text{CH}_2$), 2.5 (2H, *d*, equatorial $(\text{SCH}_2)_2\text{CH}_2$), 2.65 (1H, *dt*, equatorial $(\text{SCH}_2)_2\text{CH}_2$), 2.78 (4H, *m*, $\text{PCH}_2\text{CH}_2\text{P}$), 7.5–8.0 (20H, *m*, C_6H_5). ^{31}P NMR (202 MHz, CD_2Cl_2): δ 71. $^{13}\text{C}\{^1\text{H}\}$ NMR (19 °C, CD_2Cl_2 , 150 MHz): δ 26, 36 (s, 2:1, *pdt* CH_2); 30 (*t*, $J_{\text{PC}} \approx {}^2J_{\text{PC}} = 10$ Hz, $\text{PCH}_2\text{CH}_2\text{P}$); 130, 134, 134.5 (PPH_n); 204 (s, $\text{Fe}(\text{CO})_3$), 205 (s, $\text{Fe}(\text{CO})_3$). FT-IR (CH_2Cl_2): $\nu_{\text{CO}} = 2082, 2024 \text{ cm}^{-1}$. Anal. Calcd for $\text{C}_{32}\text{H}_{31}\text{BF}_4\text{FeNiO}_3\text{P}_2\text{S}_2$ (found): C, 50.10 (50.16); H, 4.55 (4.75). Single crystals of $[\text{1H}]\text{BF}_4 \cdot \text{CH}_2\text{Cl}_2$ were grown from CH_2Cl_2 -ether.

Reaction of 1 with B(C₆F₅)₃ and H₂. Under an inert atmosphere 4.0 mg $\text{B}(\text{C}_6\text{F}_5)_3$ (0.0078 mmol) and 6.6 mg (0.0094 mmol) of **1** was dissolved with 0.5 mL of CD_2Cl_2 in a J. Young NMR tube. The ^1H and $^{31}\text{P}\{^1\text{H}\}$ NMR spectra were recorded initially showing 16% conversion to the hydride $[\text{1H}]^+$, which we attribute to the action of $(\text{H}_2\text{O})\text{B}(\text{C}_6\text{F}_5)_3$. Spectra recorded after 1 h verified that no change occurred. The sample was then frozen and put under an H_2 atmosphere. ^1H and $^{31}\text{P}\{^1\text{H}\}$ NMR spectra showed nearly complete conversion to $[\text{1H}]^+$.

[HNiFe(pdt)(dppe)(P(OPh)₃)(CO)₂]BF₄, [2H]BF₄. To a 250-mL round bottomed Schlenk flask was dissolved 1.245 g (1.58 mmol) of $[\text{2H}]\text{BF}_4$ in 40 mL of CH_2Cl_2 . To this solution, 414 μL (1.58 mmol) of $\text{P}(\text{OPh})_3$ was added and the mixture was stirred for 6 h at 35 °C. Solvent was then removed under vacuum, and the product was extracted into a small amount of warm EtOH. Cooling of this extract to -78 °C precipitated the red product. This process was repeated 3 \times followed by recrystallization of the material from an EtOH solution by the addition of hexane. Yield: 1.06 g (1.0 mmol, 62%). ^1H NMR (400 MHz, CD_2Cl_2): δ 6.6–8.0 (35H, *m*, $\text{Ph}'\text{s}$), 2.88–1.1 ($\text{PCH}_2\text{CH}_2\text{P}$, $\text{SCH}_2\text{CH}_2\text{CH}_2\text{S}$), -3.45 (1H, *dt*, $\text{Ni}(\mu\text{-H})\text{Fe}$). $^{31}\text{P}\{^1\text{H}\}$ NMR (161 MHz, CD_2Cl_2): δ 161 (s, $\text{P}(\text{OPh})_3$), 65.8 (br, *dppe*). FT-IR (CH_2Cl_2): $\nu_{\text{CO}} = 2031, 1981 \text{ cm}^{-1}$.

[HNiFe(pdt)(dppe)(PPh₃)(CO)₂]BF₄, [3H]BF₄. Method A. To a 100-mL round bottomed Schlenk flask fitted with magnetic stir bar was added 0.126 g (0.180 mmol) of $\text{NiFe}(\text{pdt})(\text{dppe})(\text{CO})_3$ from the glovebox and dissolved in 25 mL of CH_2Cl_2 . To this green solution 0.077 g of (0.220 mmol) $[\text{HPPH}_3]\text{BF}_4$ and 0.105 g (0.400 mmol) of PPh_3 were added. After 3.5 h photolysis with a Spectroline black light lamp (365 nm), the FT-IR spectrum showed complete consumption of $[\text{1H}]\text{BF}_4$. The solution was then concentrated under vacuum and addition of 40 mL of Et_2O provided a red precipitate. The product was washed with 3×10 mL of Et_2O , and dried under vacuum. Yield: 0.113 g (0.121 mmol, 67%).

Method B. To a 250-mL round bottomed flask fitted with magnetic stir bar was prepared a solution of 0.262 g (0.333 mmol) of $[\text{1H}]\text{BF}_4$ in 50 mL of THF. To this solution 0.98 g (3.74 mmol) of PPh_3 was added. After stirring the solution for 2 h at 40 °C, the solvent was removed in vacuum yielding a red colored oil, which was washed with four 20-mL portions of hexane. The remaining oil was redissolved in 30 mL of CH_2Cl_2 , and the microcrystalline product was precipitated by addition of 100 mL of hexane. Yield: 0.235 g (0.230 mmol, 70%). ^1H NMR (400 MHz, CD_2Cl_2): δ 6.8–7.9 (35H, *m*, C_6H_5), 2.7 (4H, *m*, $\text{PCH}_2\text{CH}_2\text{P}$), 2.7–1.4 (6H, *m*, $\text{SCH}_2\text{CH}_2\text{CH}_2\text{S}$), δ -3.08 (1H, *dt*, $\text{Ni}(\mu\text{-H})\text{Fe}$). $^{31}\text{P}\{^1\text{H}\}$ NMR (161 MHz, CD_2Cl_2): δ 69.5 (s, PPh_3), 65.8 (br, *dppe*). $^{13}\text{C}\{^1\text{H}\}$ NMR (19 °C, CD_2Cl_2 , 150 MHz): δ 25.0, 25.75, 36.2 (s, 1:1:1, *pdt* CH_2 's); 28.6 (br, $\text{PCH}_2\text{CH}_2\text{P}$); 128–134 (m br, PPH_n); 211 (br, $\text{Fe}(\text{CO})_2$). $^{13}\text{C}\{^1\text{H}\}$ NMR (-60 °C, CD_2Cl_2 , 150 MHz): δ 24.95, 25.56, 36.62 (*pdt* CH_2 's), 27.98 + 29.18 (br, *dppe* $\text{PCH}_2\text{CH}_2\text{P}$), 128–134 (m br, C_6H_5), 211.2 + 211.6 (br, $\text{Fe}(\text{CO})_2$). FT-IR (CH_2Cl_2): $\nu_{\text{CO}} = 2016, 1964 \text{ cm}^{-1}$. Anal. Calcd for $\text{C}_{49}\text{H}_{46}\text{BF}_4\text{FeNiO}_2\text{P}_3\text{S}_2$ (found): C, 57.40 (57.48); H, 4.52 (4.36).

NiFe(pdt)(dppe)(PPh₃)(CO)₂, 3. In a 100-mL round-bottomed Schlenk flask was dissolved 0.110 g (0.107 mmol) of $[\text{3H}]\text{BF}_4$ in 5 mL of CH_2Cl_2 and 2 mL of MeOH. To this red solution 5.8 mg (0.107 mmol) of NaOMe was added. After stirring for 3 h, the

- (44) Gálvan, I. F.; Volbeda, A.; Fontecilla-Camps, J. C.; Field, M. J. *Proteins: Struct., Funct., Bioinf.* **2008**, *73*, 195–203.
 (45) Pershad, H. R.; Duff, J. L. C.; Heering, H. A.; Duin, E. C.; Albracht, S. P. J.; Armstrong, F. A. *Biochemistry* **1999**, *38*, 8992–8999.
 (46) Connelly, N. G.; Geiger, W. E. *Chem. Rev.* **1996**, *96*, 877–922.
 (47) Leger, C.; Jones, A. K.; Roseboom, W.; Albracht, S. P. J.; Armstrong, F. A. *Biochemistry* **2002**, *41*, 15736–15746.
 (48) Hartwig, J. F. *Organotransition Metal Chemistry, from Bonding to Catalysis*; University Science Books: New York, 2010. Drent, E.; Arnoldy, P.; Budzelaar, P. H. M. *J. Organomet. Chem.* **1994**, *475*, 57–63.
 (49) Rakowski DuBois, M.; DuBois, D. L. *Chem. Soc. Rev.* **2009**, *38*, 62–72. Barton, B. E.; Olsen, M. T.; Rauchfuss, T. B. *J. Am. Chem. Soc.* **2008**, *130*, 16834–16835. Grotjahn, D. B. *Chem.—Eur. J.* **2005**, *11*, 7146–7153. Grotjahn, D. B. *Pure Appl. Chem.* **2010**, *82*, 635–647.
 (50) Li, P.; Wang, M.; Chen, L.; Liu, J.; Zhao, Z.; Sun, L. *Dalton Trans.* **2009**, 1919–1926.

reaction mixture was evaporated under vacuum. The residue was washed with H₂O (3 × 5 mL) and MeOH (3 × 5 mL), and the green powder was dried under vacuum. Yield: 74 mg (0.079 mmol, 74%). ¹H NMR (400 MHz, CD₂Cl₂): δ 7.2–8.0 (35H, *m*, C₆H₅), 2.1 (4H, *m*, PCH₂CH₂P), 1.8–0.8 (6H, *m*, SCH₂CH₂CH₂S). ³¹P{¹H} NMR (161 MHz, CD₂Cl₂): δ 55 (*t*, PPh₃), 45 + 77 (*br*, dppe). FT-IR (CH₂Cl₂): ν_{CO} 1971, 1916 cm⁻¹. Anal. Calcd for C₄₉H₄₅FeNiO₂P₃S₂ (found): C, 62.10 (62.78); H, 4.78 (4.45).

[HNiFe(pdt)(dppe)(PPh₂Py)(CO)₂]BF₄ ([4H]BF₄) and its Protonation. To a 250-mL round-bottom Schlenk flask was added 0.400 g [1H]BF₄ (0.508 mmol) and dissolved in 30 mL THF. To this solution 0.150 g (0.570 mmol) of Ph₂PyP was added. After stirring the solution for 3 h at 40 °C, solvent was concentrated, and the product was precipitated by addition of Et₂O. The red solid was recrystallized from 15 mL of acetone by the addition of 60 mL of EtOAc. The red microcrystalline material was dried under vacuum and stored in the glovebox. Yield: 0.309 g (0.302 mmol, 59%). ¹H NMR (500 MHz, CD₂Cl₂): δ 6.8–7.9, 8.8 (35H, *m*, C₆H₅, C₅H₄N), δ 862 (4H, *m*, PCH₂CH₂P), δ 2.53–1.49 (6H, *m*, SCH₂CH₂CH₂S), δ 3.19 (1H, *dt*, Ni(μ-H)Fe). ³¹P{¹H} NMR (202 MHz, CD₂Cl₂): δ 73.7 (*s*, PPh₂Py), 65.7 (*br*, dppe). FT-IR (CH₂Cl₂): ν_{CO} = 2022, 1971 cm⁻¹. Samples of [4H₂]²⁺ were generated by protonation of degassed CH₂Cl₂ solutions with ~5 equiv of CF₃CO₂H, however the resulting dication was observed to decompose over the course of minutes. The decomposition mixture consisted of [1H]BF₄, Ni(pdt)(dppe), and [HPPH₂Py]⁺ as indicated by ³¹P{¹H} and ¹H NMR spectra. ¹H NMR (400 MHz, CD₂Cl₂): δ 7.2–7.8 (*m*), 8.0 (*t*), 8.3 (*t*), 8.8 (*d*) (35H, C₆H₅, C₅H₄N), δ 86 (4H, *m*, PCH₂CH₂P), δ 2.7–1.5 (6H, *m*, SCH₂CH₂CH₂S), δ 914 (1H, *dt*, Ni(μ-H)Fe). ³¹P{¹H} NMR (161 MHz, CD₂Cl₂): δ 79 (*s*, PPh₂Py), 66 (*br*, dppe). FT-IR (CH₂Cl₂): ν_{CO} = 2032, 1982 cm⁻¹.

pK_a Determination of [3H]BF₄. In a J. Young NMR tube, 0.8 mL dry degassed PhCN was added to 10.0 mg (0.0098 mmol) of [3H]BF₄. To this solution 197 μL of a freshly prepared solution of 0.197 M of 4-methoxyppyridine in PhCN (pK_a^{MeCN} = 14.23)²⁵ was added. The ³¹P NMR spectrum was then recorded after 1, 2, 3, and 5 h. At each interval the ratio of 3:[3H]⁺ remained unchanged at 2:1, despite steady decomposition of the sample. The ratio was determined by integration of the respective PPh₃ signals.

pK_a Determination of [1H]BF₄. In a 25 mL Schlenk flask, 4 mL dry degassed PhCN was added to 5.8 mg (0.0073 mmol) of [1H]BF₄. To this solution was added 27.6 μL of a freshly prepared solution of 0.5 M of aniline in PhCN (pK_a^{MeCN} = 10.7).²⁵ The FT-IR spectrum was then recorded after 3, 8, and 18 h. At each interval the ratio of 1:[1H]⁺ remained unchanged at 1:1.

H/D Exchange of [3H]BF₄ with D₂O. Under an inert atmosphere 4.3 mg (0.0042 mmol) of [3H]BF₄ was dissolved with 0.5 mL *d*₆-acetone (ampule, Cambridge) in a J. Young NMR tube. A ¹H NMR spectrum was recorded for *t* = 0, then 10 μL (0.56 mmol) D₂O was added (in air) and subsequent scans were collected by at 2 min intervals. The intensity of the μ-H signal (δ -3.08), determined vs phenyl region, decayed in a first order manner. After the complete disappearance of the hydride signal for [3H]BF₄, a ³¹P{¹H} spectrum was recorded, verifying the presence of the deuteride ([3D]BF₄) with no decomposition.

H/D Exchange of [4H]BF₄ with D₂O. A solution of 7.2 mg (0.00705 mmol) of [4H]BF₄ in 0.5 mL of *d*₆-acetone was prepared in a J. Young NMR tube. The ¹H NMR spectrum was recorded for *t* = 0. The sample was then frozen, 10 μL (0.56 mmol) of D₂O was added, and the sample tube evacuated and then the sample thawed. The ¹H NMR spectrum was recorded 5 min after thawing the sample, showing nearly complete consumption of the hydride

signal (δ -3.19). A ³¹P{¹H} spectrum verified the presence of the deuteride complex ([4D]BF₄) with no decomposition.

Kinetics of Deprotonation of [3H]BF₄ with NEt₃. In a J. Young NMR tube, a solution of 5.4 mg (0.0052 mmol) of [3H]BF₄ in 0.5 mL of CD₂Cl₂ was treated with 12 μL (0.086 mmol) of NEt₃ added by syringe. The tube was then sealed, and ¹H and ³¹P{¹H} NMR spectra were recorded. The first-order decay plot was constructed from ³¹P{¹H} NMR spectra, as the ratio of 3/[3H]BF₄ could be readily determined by integration of the respective PPh₃ signals. The ¹H NMR data confirm the pseudofirst order behavior.

Electrochemistry, General Considerations. As the nickel–iron hydrides presented in this paper degrade over the course of minutes in MeCN solution, electrochemistry was mainly performed on CH₂Cl₂ solutions. Cyclic voltammetry experiments were carried out in a 20-mL one compartment glass cell with tight-fitting Teflon lid with three tight-fitting electrodes and nitrogen gas inlet, interfaced with a BAS-100 Electrochemical Analyzer. The working electrode was a glassy carbon disk (diameter: 0.3 cm). A silver wire was used as a pseudoreference electrode, and the counter electrode was a Pt wire. The electrolyte was 0.1 M Bu₄NPF₆ in CH₂Cl₂. Ferrocene was added as an internal reference and cyclic voltammograms were each referenced to this Fc^{0/+} couple (0.00 V). *i*R compensation was applied: solutions were pulsed prior to each scan to determine the cell resistance, this compensation was applied to the subsequent voltammogram. Between scans electrodes were polishing with alumina.

Overpotentials are estimated from the potential at 0.5(*i*_{pc}) where *i*_{pc} is the peak current in the acid-independent regime (see Figure 11). Using the acidity constant for CF₃CO₂H (TFA) in MeCN solution, pK_{TFA}^{MeCN}, of 12.65 (and ignoring homoconjugation),²⁵ E⁰_{TFA/H₂} was calculated using Evans' relationship (eq 5).²⁶

$$E_{\text{TFA}}^0 = E_{\text{H}^+}^0 - (2.303RT/F)pK_{\text{TFA}}^{\text{MeCN}} = -0.89 \text{ V} \quad (5a)$$

Cyclic Voltammetry for [2H]BF₄ and 2. A solution of 2.6 mg (0.00243 mmol) of [2H]BF₄ in 5 mL of CH₂Cl₂ was prepared in the CV cell and was treated with successive aliquots (18 μL, 2 equiv) of freshly prepared 0.268 M CF₃CO₂H–CH₂Cl₂ solution. A solution of 5.9 mg (0.0055 mmol) of [2H]BF₄ in 3.0 mL of MeCN (1.7 mM) with 0.1 M [NBu₄]PF₆ was prepared in the CV cell. Cyclic voltammograms were then recorded between 100–1000 mV/s. A solution of 5.1 mg (0.0052 mmol) of 2 in 2.7 mL of MeCN and 0.3 mL of CH₂Cl₂ (1.683 mM) with 0.1 M [NBu₄]PF₆ was prepared in the CV cell. Cyclic voltammograms were then recorded between 100–1000 mV/s.

Cyclic Voltammetry for [4H]BF₄. A solution of 3.8 mg (0.0037 mmol) of [4H]BF₄ in 5 mL of CH₂Cl₂ was prepared in the CV cell and was treated with successive aliquots (27.7 μL, 2 equiv) of a freshly prepared solution of 0.268 M CF₃CO₂H in CH₂Cl₂ solution. Cyclic voltammograms were recorded at 100 mV/s. To determine the order with respect to [4H]BF₄, a solution of 145 μL of CF₃CO₂H in 5 mL of CH₂Cl₂ was prepared in the CV cell and treated with successive amounts of solid [4H]BF₄. The result of this titration indicated that the rate of catalysis is first-order with respect to [4H]BF₄.

Acknowledgment. This research was sponsored by NIH. We thank Dr. Danielle Gray for the crystallographic analysis of [3H]BF₄.

Supporting Information Available: Spectra, electrochemical data, and illustrative calculations. Crystallographic information file (cif) for [3H]BF₄. This material is available free of charge via the Internet at <http://pubs.acs.org>.

JA105312P